Superrotation Induced by Critical-Level Absorption of Gravity Waves on Venus: An Assessment

ARTHUR Y. HOU* AND BRIAN F. FARRELL

Center for Earth and Planetary Physics, Harvard University, Cambridge, MA 02138

(Manuscript received 31 March 1986, in final form 21 October 1986)

ABSTRACT

Critical-level absorption of a continuous spectrum of vertically propagating gravity waves is proposed as the mechanism for supporting the superrotation in the deep Venus atmosphere (below the cloud deck). It is shown that the observed westerly zonal wind effectively separates regions where waves of opposite phase speeds are absorbed, leading to westerly mean-flow acceleration below the clouds and easterly above. Using the diagnostic results of Hou and Goody, we obtain a quantitative assessment of the required wave spectrum and fluxes of energy and momentum, and show that they are compatible with observational constraints.

1. Introduction

The *Pioneer Venus* results have established that "westerly" winds (in the direction of the planetary rotation) prevail from the cloud tops (65 km) to at least a scale height above the surface; they build from about 1 m s^{-1} at 10 km to 50 m s^{-1} at the cloud base (45 km) and reach over 100 m s^{-1} at the cloud tops (Schubert, 1983). Thus, unlike the earth's atmosphere where zonal winds of both signs appear at most heights, the bulk of the Venus atmosphere "superrotates" relative to the solid planet. Ever since the discovery that the period of rotation at the cloud level is approximately 4 days compared to 243 days at the surface, the cause of this rapid superrotation has been the subject of theoretical speculations. Proposed schemes include the "moving flame" or tidal mechanism (Schubert and Whitehead, 1969; Young and Schubert, 1973; Malkus, 1970; Thompson, 1970; Fels and Lindzen, 1974), solar gravitational torque due to the semidiurnal thermal tide (Gold and Soter, 1971), and Kelvin waves (Covey and Schubert, 1982); however, none of these has been demonstrated to be diagnostically consistent with the atmospheric structure as we now know it.

Recently, using *Pioneer Venus* data Hou and Goody (1985) have performed a diagnostic model study to determine the zonally averaged eddy sources for maintaining the observed zonal wind field. Their results suggest that in the cloud region, where most of the solar heating is deposited, the zonal wind structure could be sustained by the mean meridional transport and an eddy source pattern attributable partially to atmospheric tides, while below the clouds eddy sources are needed to offset the small-scale diffusion indicated by in situ measurements. The purpose of this paper is to examine the possibility that the superrotation below the cloud deck may be maintained by critical-level absorptions of gravity waves. Although there is little quantitative data on gravity waves in the Venus atmosphere, their presence is evident in recent data, as discussed in Schubert (1983), Schubert and Waltersheid (1984), and Linkin et al. (1986).

The mechanism proposed here is similar in concept to that for the quasi-biennial oscillation (QBO) in the earth's stratosphere (Lindzen and Holton, 1968; Plumb, 1977). However, in the atmosphere of Venus, due to the ubiquitous westerlies, only waves with westerly phase speeds encounter critical levels. In this work we show that for the observed Venus structure, the absorption of waves with westerly phase speeds at critical levels could provide the necessary westerly acceleration to balance the diffusive loss, while waves with easterly phase speeds are nearly trapped but could lead to easterly acceleration through breaking or thermal damping above the cloud base. Thus, the presence of westerlies in the Venus atmosphere effectively separates regions where waves of opposite phase speeds are absorbed, with easterly wave momentum flux deposited in a region where the mean meridional motion, thermal tides, and possibly other processes all play an important role in determining the zonal wind structure.

Assuming that the zonal momentum of the mean flow is balanced by diffusion below the cloud base, as suggested by the model result of Hou and Goody (1985), we invert for the gravity wave spectrum required for supporting the zonal wind below 45 km. We show that vertical transports of momentum and energy by westerly waves significantly exceeds those by easterly waves, that the total wave energy flux corresponds to a small fraction of the solar flux reaching the ground, and that easterly waves could play an important role in reversing the vertical wind shear above 80 km. We

* Also affiliated with Atmospheric and Environmental Research, Inc., Cambridge, MA 02139.

will examine these results in the light of available observational constraints, and lastly, discuss penetrative convection as a possible mechanism for exciting gravity waves near the planet surface.

The basic equations are described in section 2, model parameters are given in section 3, the results are presented in sections 4 and 5, sensitivities are tested in section 6, and an overall assessment is given in section 7.

2. The model concept

a. Gravity waves due to a unit forcing

As a simple framework for illustrating the proposed mechanism, we consider two-dimensional, inviscid, hydrostatic gravity waves for equatorial applications and assume that the effect of the small planetary rotation rate is negligible on the gravity wave time scale. From Holton (1975), the linearized perturbation equations in log-pressure coordinates are:

$$\left.\begin{aligned} u_t+\bar{u}u_x+\bar{u}_\zeta w+\phi_x&=0\\ \frac{R}{H}(T_t+\bar{u}T_x)+N_*^2 w&=-\frac{R}{H}\frac{T}{\tau}\\ u_x+\frac{1}{\rho_*}(\rho_* w)_\zeta&=0\\ \phi_\zeta&=\frac{RT}{H} \end{aligned}\right\}, \quad (1)$$

where

$$H=\frac{RT_s}{g}$$

$$\zeta=-H\ln\left(\frac{p}{p_s}\right)$$

$$w=\frac{D\zeta}{Dt}$$

$$\rho_*=\rho_s\exp\left(-\frac{\zeta}{H}\right)$$

$$N_*^2=\frac{R}{H}\left(\bar{T}_\zeta+\frac{R}{c_p}\frac{\bar{T}}{H}\right);$$

where subscripts t, x and ζ denote partial derivatives with respect to time, zonal and "vertical" axes; u and w are perturbation zonal and "vertical" velocities, respectively; ϕ is the perturbation geopotential height, T is the perturbation temperature, and $\tau(\zeta)$ is the thermal relaxation time. The basic state is defined by the time-zonal-mean profiles of zonal wind and temperature, $\bar{u}(\zeta)$ and $\bar{T}(\zeta)$, with no mean vertical motion $\bar{w}$. We assume a perfect-gas, CO_2 atmosphere with a gas constant R and a constant heat capacity c_p; g is the gravitational acceleration, the subscript s denotes a reference value at the planet surface, and $N_*(\zeta)$ is related to the Brunt–Väisälä frequency $N(\zeta)=[g/T_s(d\bar{T}/dz+g/c_p)]^{1/2}$ by

$$\frac{N_*(\zeta)}{N(\zeta)}=\frac{dz}{d\zeta}=\frac{\bar{T}(\zeta)}{T_s}, \quad z=\text{physical height}, \quad (2)$$

and the basic state density $\bar{\rho}$ is given by

$$\frac{\bar{\rho}(\zeta)}{\rho_*(\zeta)}=\frac{T_s}{\bar{T}(\zeta)}. \quad (3)$$

For any variable X (i.e., u, w, T, or ϕ), we seek a solution of the form $\hat{X}(\zeta)\exp[ik(x-ct)]$ due to a steady, periodic excitation at some level ζ_0; the notations are standard and the wave frequency is $-kc$. From (1) we obtain the vertical structure equation:

$$\hat{W}_{\zeta\zeta}(\zeta)+Q(\zeta,c)\hat{W}(\zeta)=0, \quad (4)$$

where $\hat{W}(\zeta)=\tilde{W}(\zeta)\exp[-(\zeta-\zeta_0)/2H]$, and $Q(\zeta, c)$ is the index of refraction,

$$Q(\zeta,c)=\frac{N_*^2}{(\bar{u}-c)(\bar{u}-c-i/k\tau)}-\frac{\bar{u}_{\zeta\zeta}+\bar{u}_\zeta/H}{\bar{u}-c}-\frac{1}{4H^2}.$$

Given values of k and c, (4) can be solved using the Lindzen–Kuo algorithm for a unit $\hat{W}$ forcing at ζ_0 and a radiation condition applied at the model top (e.g., Lindzen and Barker, 1985). The solution for w then has the form

$$w=\exp[(\zeta-\zeta_0)/2H]\,\mathrm{Re}\{\hat{W}(\zeta)\exp[ik(x-ct)]\}, \quad \zeta\geq\zeta_0. \quad (5)$$

Substituting (5) into (1) leads to

$$u=k^{-1}\exp[(\zeta-\zeta_0)/2H]\times\mathrm{Re}\left\{i\left(\hat{W}_\zeta-\frac{\hat{W}}{2H}\right)\exp[ik(x-ct)]\right\},$$

$$T=k^{-1}\frac{HN_*^2}{R}\exp[(\zeta-\zeta_0)/2H]\times\mathrm{Re}\left\{\frac{i\hat{W}}{\bar{u}-c-i/k\tau}\exp[ik(x-ct)]\right\}.$$

$$\phi=k^{-1}\exp[(\zeta-\zeta_0)/2H]\times\mathrm{Re}\left\{i\left[\bar{u}_\zeta\hat{W}+(\bar{u}-c)\left(\frac{\hat{W}}{2H}-\hat{W}_\zeta\right)\right]\times\exp[ik(x-ct)]\right\}. \quad (6)$$

The density-weighted vertical momentum flux averaged over a wave period is

$$\rho_*\overline{wu}=k^{-1}\frac{\rho_s}{2}\exp(-\zeta_0/H)\,\mathrm{Re}(i\hat{W}_\zeta\hat{W}^*); \quad (7)$$

where $\hat{W}^*$ is the complex conjugate of $\hat{W}$. The resulting mean-flow acceleration G is

$$G(\zeta) = -\frac{1}{\bar{\rho}(\zeta)}\frac{d}{dz}(\rho_* \overline{wu}); \quad (8)$$

the associated "vertical energy flux" is

$$\rho_* \overline{w\phi} = k^{-1}\frac{\rho_s}{2}\exp(-\zeta_0/H)\,\mathrm{Re}[-i(\bar{u}-c)\hat{W}_\zeta \hat{W}^*]; \quad (9)$$

and (7) and (9) satisfy the Eliassen–Palm relation $\rho_* w\phi = -(\bar{u} - c)\rho_* \overline{wu}$.

b. Energetics

The energetic consistency of (1) requires that the time rate of change of the total energy $E_T = \frac{1}{2}\rho_*(\overline{u^2} + \overline{(\phi_\zeta/N_*)^2} + \bar{u}^2)$ satisfy

$$\frac{\partial E_T}{\partial t} = -\frac{\partial}{\partial z}(\rho_* \overline{wuu}) - \frac{\partial}{\partial z}(\rho_* \overline{w\phi}) - \frac{\rho_*}{\tau}\overline{\left(\frac{\phi_\zeta}{N_*}\right)^2},$$

by which the total energy is conserved in the absence of forcing and boundary fluxes. Locally, a steady wave satisfies the energetic relation

$$\bar{u}\frac{d}{dz}(\rho_* \overline{wu}) - \frac{d}{dz}[\rho_*(\overline{wuu} + \overline{w\phi})] - \frac{\rho_*}{\tau}\overline{\left(\frac{\phi_\zeta}{N_*}\right)^2} = 0. \quad (10)$$

c. The continuous spectrum

In order for critical-level absorption to support the observed zonal wind profile, a continuous spectrum of gravity waves must be present. The counterparts to (7)–(9) for a continuous spectrum may be expressed as:

$$[q(z)] = \int_c \int_k A^2(k, c) q(k, c; z)\, dk dc, \quad (11)$$

where $[q]$ denotes the contribution from the spectrum to any quadratic wave quantity q, with $q(k, c; z)$ being the response to a unit forcing [e.g., (7)–(9)] and A^2 defining the spectral density of the square of the vertical velocity scaled by $\hat{W}(z_0)$. The derivation of (11) assumes that the averaging period is sufficiently long so that only self-correlations need be retained.

To determine the wave amplitude required for supporting the superrotation below the Venus clouds, we utilize the diagnostic results of Hou and Goody (1985), which show that for the amount of turbulent mixing indicated by *Pioneer Venus* measurements (i.e., $\nu \approx 1$ to 5 $m^2\ s^{-1}$, see von Zahn et al., 1983), the required momentum sources below the cloud base $z_b = 45$ km is dictated by diffusion. Substituting (8) into (11) gives the total mean-flow acceleration due to a continuous spectrum of gravity waves. Equating this with the acceleration required to offset the diffusive loss yields an equation for A^2. In the absence of data on the spectrum of zonal waves present in the Venus atmosphere, we will solve A^2 as a function of c for a single wave number k; i.e.,

$$\bar{\rho}(z)[G(z)] = -\int_{c(z_0)}^{c(z_b)} A^2(c)\frac{d}{dz}(\rho_* \overline{wu})\, dc = -\frac{d}{dz}\left(\bar{\rho}\nu\frac{d\bar{u}}{dz}\right). \quad (12)$$

where $c(z_b) = \bar{u}(z_b)$ and $c(z_0) = \bar{u}(z_0)$. The effect of the finite wave number spectrum is estimated in section 2d.

d. Required critical-layer acceleration and wave spectrum

For westerly waves with a critical level, following Hazel (1967) and Fritts and Geller (1975) we assume that the wave momentum flux is deposited by viscous stablization within a layer of thickness Δz_ν, where

$$\Delta z_\nu = \left(\frac{\nu}{k\bar{u}_z}\right)^{1/3}. \quad (13)$$

For thin critical layers and long thermal damping times (which is appropriate for Venus parameters below the cloud base, as will be shown in section 5), the momentum flux divergence term in (12) at $z = z_{CL}$ may be approximated by

$$\frac{d}{dz}(\rho_* \overline{wu}) = \begin{cases} -\rho_* \overline{wu}(k, c; z_0)/\Delta z_\nu & z_{CL} \geq z \geq z_{CL} - \Delta z_\nu \\ 0 & \text{elsewhere} \end{cases}$$

where z_{CL} denotes the height of the critical level, and the momentum flux is evaluated at z_0 since the wave is conservative until reaching the critical layer. Substituting this into (12) leads to a matrix for determining $A^2[c(z_{CL})]$. Note that since critical-layer accelerations are confined to thin layers, the contribution to the integral (12) at any $z = z_{CL}$ stems only from the interval $\Delta c = |c(z_{CL} + \Delta z_\nu) - c(z_{CL})| = |\bar{u}(z_{CL} + \Delta z_\nu) - \bar{u}(z_{CL})|$. Assuming that $A^2(c)$ and $\rho_* \overline{wu}(c)$ are smooth functions of c so that their values are approximately constant over Δc, (12) may be evaluated using the relation $\Delta c/\Delta z_\nu = \Delta\bar{u}/\Delta z_\nu = |\bar{u}_z(z_{CL})|$ to give

$$A^2[c(z_{CL})] = (\rho_* \overline{wu}(c)|\bar{u}_z(z_{CL})|)^{-1}\left[-\frac{d}{dz}\left(\bar{\rho}\nu\frac{d\bar{u}}{dz}\right)\right]_{z_{CL}}. \quad (14)$$

where $A^2(c)$ has the units of $(m\ s^{-1})^{-1}$. Evaluating (14) for $z_0 \leq z_{CL} \leq z_b$ determines the $A^2(c)$ profile for maintaining the observed zonal wind in this region. Note that under the thin-layer approximation, A^2 is *independent* of the thickness of the layer.

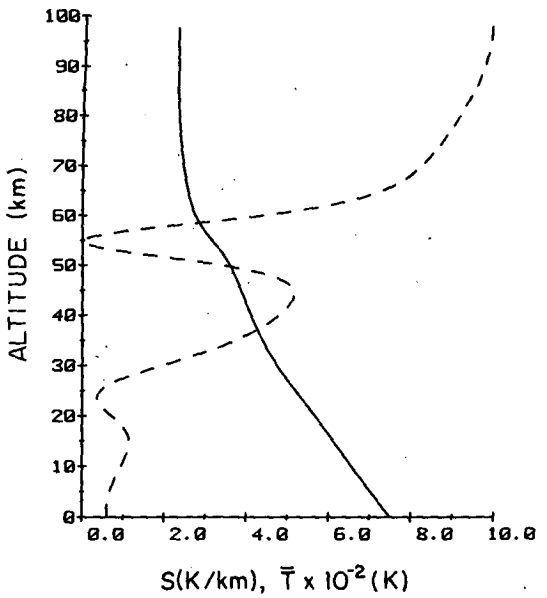

FIG. 1. Profiles of the static stability $S(z)$ (dash) and temperature $\bar{T}(z)$ (solid), as defined by (16), (17) and Table 1.

e. *Momentum deposition by easterly waves*

With the spectrum of westerly waves determined by (14), we assume that a symmetric spectrum of easterly waves is also excited. Since easterly waves do not have critical levels, they can propagate upward until breaking or absorption via thermal damping. The resulting easterly acceleration is given by (12) if damped, or in the case of breaking it may be estimated by distributing the wave momentum flux over a scale height, as in Lindzen (1980). Thus, in order for the proposed mechanism is to work, the mean-flow deceleration due to easterly waves, if deposited below the clouds, must be much smaller than the acceleration provided by the westerly waves; or if deposited above the cloud base, it must be consistent with the eddy source requirement discussed in Hou and Goody (1985).

To obtain an estimate for the amplitude of the easterly waves, we use the root-mean-square of the required forcing spectrum. Since the variance of the time series of the forcing corresponds to the integrated spectral density, the root-mean-square forcing amplitude $A_{\rm rms}$ may be defined as

$$A_{\rm rms}^2 = 2\int_{c(z_0)}^{c(z_b)} A^2(c)dc. \tag{15}$$

3. Model parameters

a. *Static stability and temperature*

The static stability $S(z) = d\bar{T}/dz + g/c_p$ is modelled from *Pioneer Venus* data (Seiff, 1983) using an analytic formula devised by Lindzen (1970); viz,

$$S(z) = \sum_{i=1}^{5} \frac{a_{i+1} - a_i}{2d_i} \operatorname{sech}^2\left(\frac{z - z_i}{d_i}\right); \tag{16}$$

the consistent temperature profile is modeled by

$$\bar{T}(z) = \bar{T}'(z) - \frac{g}{c_p} z - \bar{T}'(0) + T_s, \tag{17}$$

where

$$\bar{T}'(z) = \sum_{i=1}^{5} \frac{a_{i+1} - a_i}{2}\left[1 + \tanh\left(\frac{z - z_i}{d_i}\right)\right],$$

and the coefficient a satisfies the recursion relation

$$a_1 = 0, \quad \text{and} \quad a_i = 2\hat{a}_{i-1}d_{i-1} + a_{i-1}, \quad (i = 2, 6).$$

Figure 1 displays the standard profiles of $\bar{T}(z)$ and $S(z)$, with relevant numerical coefficients given in Table 1.

b. *Zonal wind*

The zonal wind model is taken from Schubert and Waltercheid (1984):

TABLE 1. Coefficients for thermal and zonal wind structures.

	$S(z)$ and $\bar{T}(z)$ [Eqs. (16) and (17)]			$\bar{u}(z)$ [Eq. (18)]		
i	z_i (10^3 m)	$\hat{a}_i$ (km^{-1} K)	d_i (10^3 m)	z_i (10^3 m)	b_i (s^{-1})	h_i (10^3 m)
1	0	−1	10	7	1.43×10^{-4}	2
2	10	−1	10	15	2.13×10^{-3}	2.5
3	25	−3.1	8	55	1.13×10^{-3}	2.5
4	55	−6.75	5	65	4.2×10^{-3}	2.5
5	100	10	70	72.5	0	2.5
6	—	—	—	90	-6×10^{-3}	2.5
7	—	—	—	—	0	—

$$\bar{u}(z)=\frac{b_1}{2}z+\sum_{i=1}^{6}\frac{b_{i+1}-b_i}{2}h_i\ln\left[\frac{\cosh\left(\frac{z-z_i}{h_i}\right)}{\cosh\left(\frac{z_i}{h_i}\right)}\right]; \quad (18)$$

thus,

$$\bar{u}_z(z)=b_1+\sum_{i=1}^{6}\frac{b_{i+1}-b_i}{2}\left[1+\tanh\left(\frac{z-z_i}{h_i}\right)\right],$$

$$\bar{u}_{zz}(z)=\sum_{i=1}^{6}\frac{b_{i+1}-b_i}{2h_i}\operatorname{sech}^2\left(\frac{z-z_i}{h_i}\right).$$

Figure 2 gives the adopted $\bar{u}(z)$ profile with the numerical coefficients provided in Table 1.

Also plotted in Fig. 2 is the mean-flow acceleration profile required for balancing diffusion, whose structure is completely specified by $\bar{u}(z)$ and $\bar{\rho}(z)$ according to the right side of (12).

c. Thermal damping

The thermal relaxation times are fitted to the values given in Table 2 of Pollack and Young (1975):

$$\frac{\tau(z)}{\tau(0)}=\exp\left[\alpha_1-\alpha_2\left(\frac{\zeta}{H}-\alpha_3\right)\right]. \quad (19)$$

where ζ is the log-pressure height defined in (1), $\tau(0) = 1.32 \times 10^9$ seconds, and the coefficients are: $\alpha_1 = 0$, $\alpha_2 = 0.9$, $\alpha_3 = 0$, for $\zeta/H \leqslant 5$; $\alpha_1 = -4.5$, $\alpha_2 = 2$, $\alpha_3 = 5$, for $5 < \zeta/H \leqslant 7$; $\alpha_1 = -8.5$, $\alpha_2 = 0.5$, $\alpha_3 = 7$, for $\zeta/H > 7$.

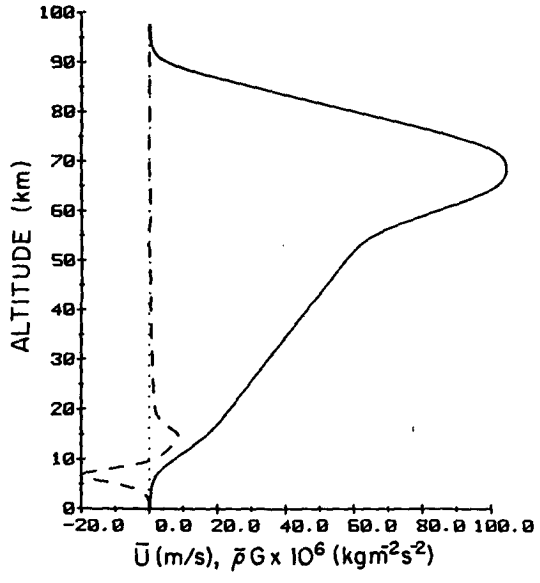

FIG. 2. The zonal wind $\bar{u}(z)$ (solid) and the mean-flow acceleration $\bar{\rho}G(z)$ required to balance diffusion (dash). The zonal wind in m s^{-1} is defined by (18) and Table 1; the acceleration in units of kg m^{-2} s^{-2} is evaluated according to the right side of (12) and scaled by $10^{-6}\bar{\rho}$.

Since the above thermal damping eventually kills the N_*^2 term in (4) above 100 km, we assume S ($z > 100$ km) = S (100 km). Similarly, we take $\bar{u}$ ($z > 100$ km) = $\bar{u}$ (100 km), as there is no information on the mean wind above this level.

Other numerical constants adopted for the model problem are: $g = 8.6$ m s^{-2}, $R = 190$ m^2 s^{-2} K^{-1}, $c_p = 860$ m^2 s^{-2} K^{-1} for a perfect-gas, CO_2 atmosphere, and $T_s = 750$ K.

4. Results for a unit forcing

a. The structure of westerly waves

In order for the critical-layer absorption of gravity waves to support the superrotation below the cloud deck ($z < 45$ km), westerly phase speeds ranging from a few meters per second to about 50 m s^{-1} (the zonal velocity at the cloud base) must be present to provide the required acceleration from $z \approx 10$ to 45 km, as shown in Fig. 2. We accordingly assume that waves are excited at $z_0 = 10$ km, i.e., in the lowest scale height (even though this may not be the only region of excitation, see Schubert, 1983). Below the clouds thermal relaxation times given by (19) are long, so that the damping term in (4) is negligible and the waves are essentially nondissipative outside critical layers and $\hat{W}(z)$ is consequently independent of k. For phase speeds with critical levels below the cloud base and frequencies less than the mean Brunt–Väisälä frequency of this region, the hydrostatic assumption, i.e., $k^2(\bar{u}-c)^2 \ll N^2$, restricts model zonal wavelengths to approximately 500 km or longer. We will perform calculations for a single 1000 km wave, as proposed in section 2c. The system (4)–(9) is solved for a unit forcing $\hat{W}(\zeta_0) = 1$ m s^{-1}. The critical-level singularity is treated numerically by introducing a small value in the imaginary part of the phase speed c_i, as in Lindzen and Barker (1985). Numerical convergence is verified by increasing the vertical resolution and by reducing the value of c_i. The standard results presented here are obtained with 8000 vertical levels and $c_i = 0.01$.

Results have been obtained for $c_r = \mathrm{Re}(c)$ greater than $\bar{u}(z_0) \approx 7.6$ m s^{-1} and less than 60 m s^{-1}. For a 1000 km wave, the corresponding periods range from 5 to 36 hours (note that Venus' period of rotation is 243 days). The basic structure of these waves are similar and is illustrated in Figs. 3 through 5 for $c_r = 40$ m s^{-1}. Figure 3 shows that the index of refraction $Q(z)$ is positive below the critical level and is dominated by the N_*^2 term. Figures 4a and 4b display the magnitudes and phases of $\tilde{W}$, $\tilde{U}$, $\tilde{T}$ and $\tilde{\Phi}$, respectively. The wave propagates upward until absorbed at the critical level at about 34.4 km. At the forcing level, the values for $\tilde{W}$, $\tilde{U}$, $\tilde{T}$ and $\tilde{\Phi}$ according to (5) and (6) are: 1 m s^{-1}, 30.8 m s^{-1}, -1.28×10^{-3} K, and 9.96×10^2 m^2 s^{-2},

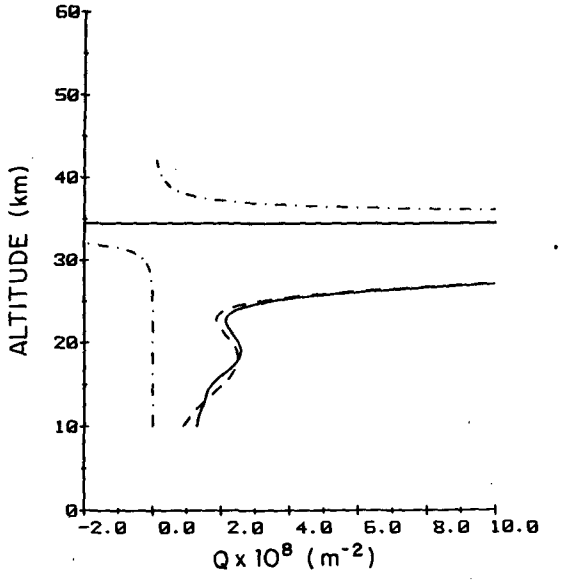

FIG. 3. The index of refraction $Q(z)$ for $c_r = 40$ m s^{-1}. The solid line shows Re(Q), which vanishes at the critical level at $z \approx 34.5$ km. The dashed show the real part of the N_*^2 term in (4), and the dash-dots are Im(Q).

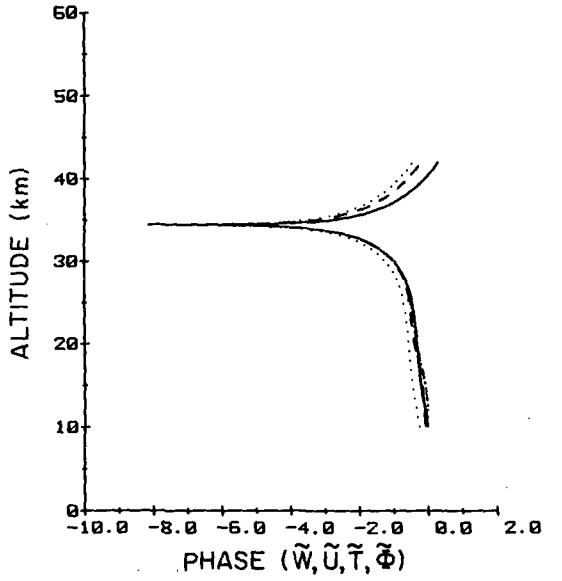

FIG. 4b. The corresponding phases of $\tilde{W}(z)$, $\tilde{U}(z)$, $\tilde{T}(z)$, and $\tilde{\Phi}(z)$ ($c_r = 40$ m s^{-1}). The legends are the same as for Fig. 4a; the values are scaled by 2π.

respectively. Note also that w and T are essentially in quadrature as for a conservative wave; this is consistent with Fig. 5 which shows that the effect of thermal damping is negligible and the wave energetics involve only the first two terms of (10). The momentum and energy fluxes of these waves are discussed in section 4c.

b. *The structure of easterly waves*

Results for the easterly waves are qualitatively different from those for the westerly waves. Without a critical level, an easterly wave can propagate to great heights and is eventually absorbed through thermal damping. For a typical easterly wave with $c_r = -40$ m

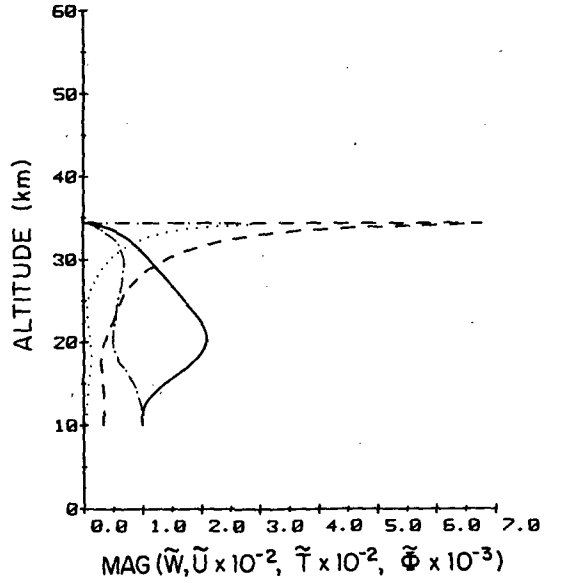

FIG. 4a. Magnitudes of $\tilde{W}(z)$, $\tilde{U}(z)$, $\tilde{T}(z)$, and $\tilde{\Phi}(z)$ due to a unit forcing at 10 km ($c_r = 40$ m s^{-1}). The solid line shows $\tilde{W}$ in m s^{-1}, the dashes are $\tilde{U} \times 10^{-2}$ in m s^{-1}, the dots are $\tilde{T} \times 10^{-2}$ in K, and the dash-dots are $\tilde{\Phi} \times 10^{-3}$ in m^2 s^{-2}.

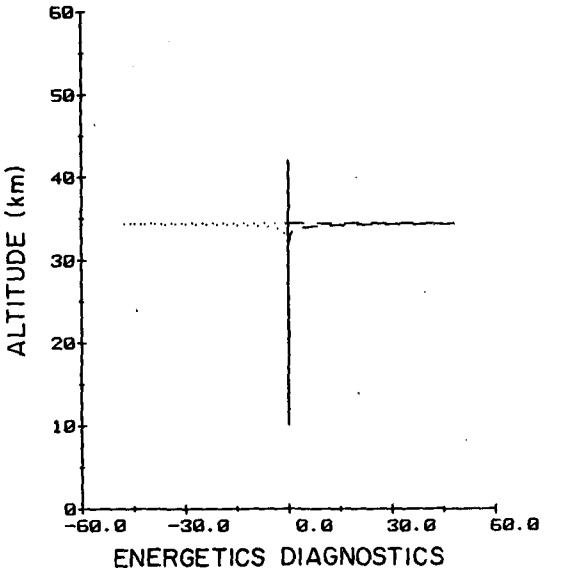

FIG. 5. Energetics for the $c_r = 40$ m s^{-1} wave according to (10). The balance is between $\bar{u}d(\rho_*\overline{wu})/dz$ (dots) and $-d[\rho_*(\overline{uwu} + \overline{w\phi})]/dz$ (dash); the effect of thermal damping (solid) is negligible. The units are W m^{-3}.

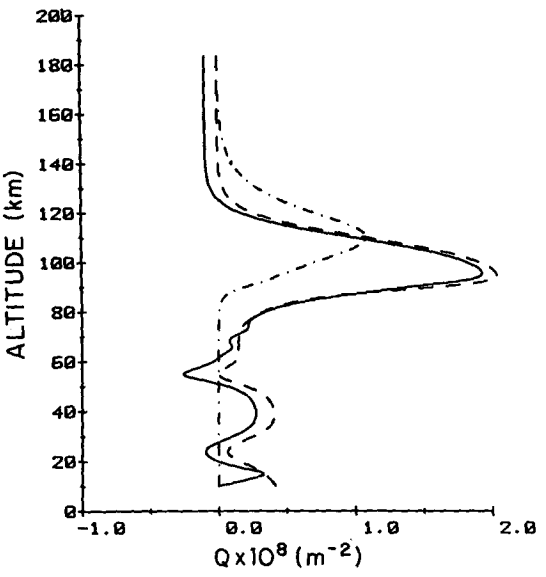

FIG. 6. The index of refraction $Q(z)$ for $c_r = -40$ m s^{-1}. The solid line shows Re(Q), the dashes show the real part of the N_*^2 term in (4), and the dash-dots are Im(Q).

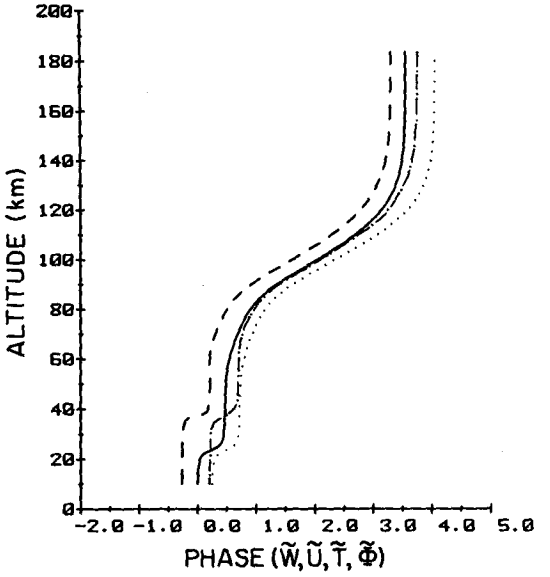

FIG. 7b. The corresponding phases of $\tilde{W}(z)$, $\tilde{U}(z)$, $\tilde{T}(z)$, and $\tilde{\Phi}(z)$ ($c_r = -40$ m s^{-1}). The legends are the same as for Fig. 7a; the values are scaled by 2π.

s^{-1}, Fig. 6 shows that the index of refraction $Q(z)$ is positive mainly in the region from 65 km to 120 km, so that the wave is evanescent or nearly so outside this region, as is evident from Fig. 7. The values of $\tilde{W}$, $\tilde{U}$, $\tilde{T}$, and $\tilde{\Phi}$ at the forcing level are 1 m s^{-1}, -1.3 m s^{-1}, -1.2×10^{-5} K, and 63.3 m^2 s^{-2}, respectively. Figure 8 shows that the perturbation energy balance (10) is between the sum of the first two terms and the thermal damping term. The resulting mean-flow deceleration due to thermal damping has a maximum at 105 km, distributed roughly with a Gaussian e-folding width of 10 km. However, the manner in which the easterly momentum flux is deposited depends on whether the wave breaks at some height (see Lindzen, 1981); this will be addressed in section 5 for wave amplitudes relevant to the Venus atmosphere.

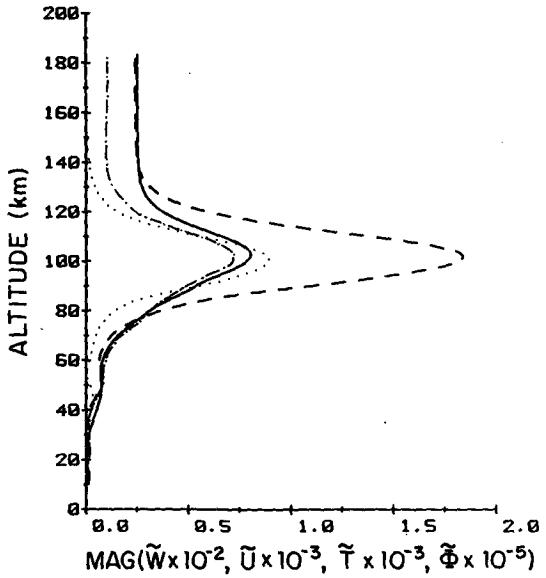

FIG. 7a. Magnitudes of $\tilde{W}(z)$, $\tilde{U}(z)$, $\tilde{T}(z)$, and $\tilde{\Phi}(z)$ due to a unit forcing at 10 km ($c_r = -40$ m s^{-1}). The solid line gives $\tilde{W} \times 10^{-2}$ in m s^{-1}, the dashes are $\tilde{U} \times 10^{-2}$ in m s^{-1}, the dots are $\tilde{T} \times 10^{-3}$ in K, and the dash-dots are $\tilde{\Phi} \times 10^{-5}$ in m^2 s^{-2}.

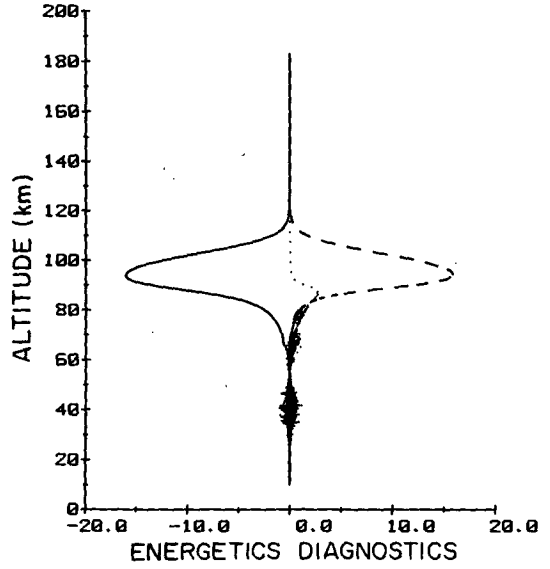

FIG. 8. Energetics for the $c_r = -40$ m s^{-1} wave according to (10). The balance is between the sum of $\bar{u}d(\rho_*\overline{wu})/dz$ (dots) and $-d[\rho_*(\overline{uwu} + \overline{w\phi})]/dz$ (dash) and the thermal damping term (solid). The units are W m^{-3}.

c. *Momentum and energy fluxes*

Figure 9 plots distributions of $\rho_* \overline{wu}$ and $\rho_* \overline{w\phi}$ at z_0 as a function of c_r. The profiles show isolated peaks due to amplifications from partially reflected waves set up by a rapidly varying $N^2(z)$, as described in Gill (1982). Such enhanced forced response has been identified with strong downslope winds induced by mountains in the earth's atmosphere (Klemp and Lilly, 1975; Lindzen and Tung, 1976; Blumen and Hartsouth, 1985). The prominent peaks in the easterly momentum profile in Fig. 9 are likely due to the trapping by the $1/4H^2$ term above 120 km, where $\bar{u}$ vanishes and the N_*^2 term is mitigated by the short thermal damping time, leading to Re $(Q) < 0$ and Im $(Q) = 0$ in this region (see Fig. 6). This is analogous to Gill's two-layer result for an evanescent wave in the upper layer and a strongly stratified lower layer (Gill, 1982, Eq. 6.9.16).

Figure 3 shows that the index of refraction for the westerly waves is always positive and attains a large magnitude just below the critical level; this is analogous to Gill's case of a weakly stratified lower layer. Thus, the resulting momentum flux profile varies approximately as $1/(\bar{u} - c)$, modulated by partially reflected waves, but does not have the singular behavior of the easterly waves.

Figure 9 shows that for most phase speeds, the energy and momentum fluxes carried by the propagating westerly waves are much greater than those by the nearly trapped easterly waves. In particular, outside the amplification regions, fluxes associated with easterly

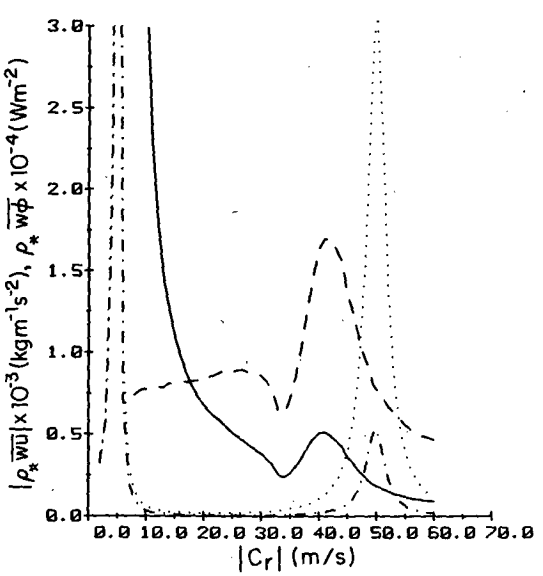

FIG. 9. Vertical fluxes of momentum and energy at z_0 for a unit forcing. The values are scaled by $\hat{k}^{-1}$. The solid curve shows $|\rho_* \overline{wu}| \times 10^{-3}$ for westerly waves in units of kg m^{-1} s^{-2} and the dash-dots are corresponding values for easterly waves. The dashes are $\rho_* \overline{w\phi} \times 10^{-4}$ for westerly waves in units of W m^{-2} and the dots are for easterly waves.

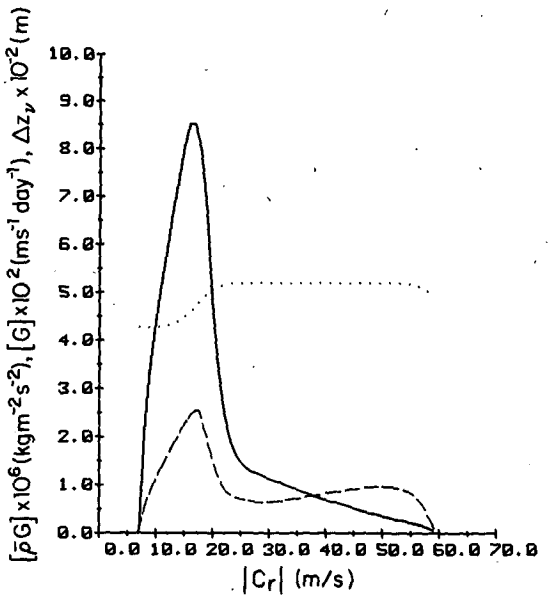

FIG. 10. The mean-flow acceleration required for balancing diffusion as a function of the critical-level phase speed. The units are kg m^{-2} s^{-2} for $[\bar{\rho}G]$ (scaled by $10^{-6}\hat{\nu}$, solid) and m s^{-1}/day for $[G]$ (scaled by $10^{-2}\hat{\nu}$, dash). Also shown is the critical layer thickness Δz_ν given in (13); the values are in meters scaled by $10^2(\hat{\nu}/\hat{k})^{1/3}$.

waves are at least one order of magnitude smaller than their westerly counterparts. The resulting east-west asymmetry due to the westerly zonal wind is therefore quite pronounced. Note that the energy flux profile for westerly waves is flat for $c_r \lesssim 30$ m s^{-1}, which confirms the $1/(\bar{u} - c)$ dependence of the westerly momentum flux at these phase speeds.

5. Results for the Venus atmosphere

The mean-flow acceleration required for balancing diffusion is given by the right-hand side of (12) and shown in Fig. 10 as a function of $c_r(z_{CL})$. Also shown is the critical layer thickness $\Delta z_\nu[c_r(z_{CL})]$ according to (13). The values are scaled by dimensionless parameters $\hat{\nu} = \nu/\nu_0$ with $\nu_0 = 1$ m^2 s^{-1}, and $\hat{k} = k/k_0$, with $k_0 = 2\pi \times 10^{-6}$ m^{-1} for a 1000 km wave, so that the plots correspond directly to the results for $\hat{\nu} = 1$ and $\hat{k} = 1$. These scalings will be used throughout the work, whenever appropriate.

For typical values of ν ranging from 1 to 5 m^2 s^{-1} for Venus applications, Fig. 10 shows that Δz_ν is between 500 and 800 m; hence the thin-layer approximation used in section 2d is justified.

a. *The inverted spectral density*

Substituting (7) into (14) gives the required spectral density for maintaining against diffusion below the cloud base:

$$A^2(c) = -\nu k\left[\bar{u}_z^{-1}\frac{d}{dz}\left(\bar{\rho}\frac{d\bar{u}}{dz}\right)\right]_{z_{CL}(c)} \times\left\{\frac{\rho_s}{2}\exp(-\zeta_0/H)\,\mathrm{Re}[i\hat{W}_\zeta(\zeta_0)\hat{W}^*(\zeta_0)]\right\}^{-1}. \quad (20)$$

Figure 11 plots $A^2(c)$ scaled by $\hat{\nu}\hat{k}$ in units of $(\mathrm{m\ s^{-1}})^{-1}$. The distribution has a maximum at about $c_r \approx 20$ m s^{-1}; for $c_r < 20$ m s^{-1}, it drops rapidly to zero at the cutoff $c_r(z_0) = 7.6$ m s^{-1}, which reflects the zero-divergence level of the diffusive flux; for $c_r > 20$ m s^{-1} the profile is to some extent modulated by enhancements from partially reflected waves but generally decreases with increasing c_r, roughly with a Gaussian e-folding width of about 10 m s^{-1}.

Given the spectral density, the integrated momentum flux $[\rho_*\overline{wu}]$, the total energy flux $[\rho_* w\phi]$, and the total perturbation energy $[E] = \{\frac{1}{2}\rho_*[\overline{u^2} + (\overline{\phi_\zeta/N_*})^2]\}$ can be evaluated using (11), (6), (7), and (9). The results are discussed below.

b. Momentum fluxes

The momentum fluxes at z_0 are shown in Fig. 11. The results show that the easterly momentum flux is negligible compared with its westerly counterpart, except in the narrow amplification region near $c_r = -50$ m s^{-1}, where they are comparable. Therefore, the system has a strong bias in favor of transporting westerly momentum upward in the presence of westerlies. The integrated westerly momentum flux over the range of phase speeds is $3.7 \times 10^{-2}\hat{\nu}$ kg m^{-1} s^{-2}, compared with the total easterly flux of $-0.6 \times 10^{-2}\hat{\nu}$ kg m^{-1} s^{-2}, giving a net upward flux of westerly momentum of $4.3 \times 10^{-2}\hat{\nu}$ kg m^{-1} s^{-2}. This corresponds to a loss of westerly wave momentum flux in the region below z_0. If we distribute this loss over the lowest 10 km, the resulting mean-flow deceleration is approximately $-4.3 \times 10^{-6}\hat{\nu}$ kg m^{-1} s^{-2}, or roughly, -0.01 m s^{-1}/day. Presumably, this is balanced by diffusion and possibly other processes such as a surface Hadley cell similar to that found by Hou and Goody (1985).

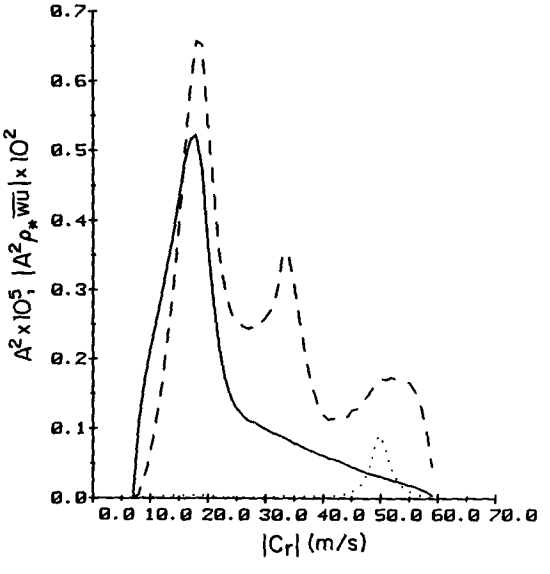

FIG. 11. The inverted spectral density $A^2(c)$ and the momentum flux profile $A^2\rho_*\overline{wu}$ at z_0. The dashes give the values of A^2 in $(\mathrm{m\ s^{-1}})^{-1}$ scaled by $10^{-5}\hat{\nu}\hat{k}$. The momentum flux density in units of kg m^{-1} s^{-2}/(m s^{-1}) is scaled by $10^{-2}\hat{\nu}$, with the solid line for westerly waves and the dashes for easterly waves.

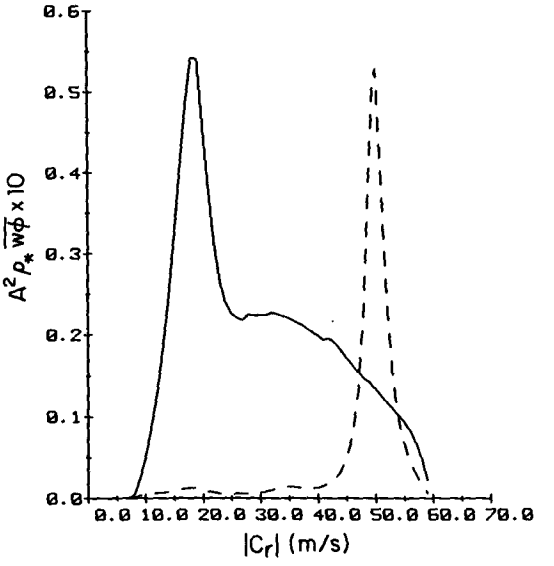

FIG. 12. The energy flux density $A^2\rho_*\overline{w\phi}$ at z_0 in units of W m^{-2}/(m s^{-1}) scaled by $10^{-1}\hat{\nu}$. The solid line is for westerly waves and the dashes for easterly waves.

c. Energetics and group velocities

Figure 12 plots the upward flux of energy $A^2\rho_*\overline{w\phi}$ at z_0. The flux carried by westerly waves is greater than that by easterly waves everywhere except in the amplification region for easterly waves. The integrated vertical energy fluxes are $0.54\hat{\nu}$ W m^{-2} for westerly waves and $0.17\hat{\nu}$ W m^{-2} for easterly waves, giving a total of $0.71\hat{\nu}$ W m^{-2} [for comparison, the value for the earth's atmosphere given by Stull (1976) is 0.1 W m^{-2}]. If these waves are indeed excited in the Venus planetary boundary layer as postulated, then the solution for $\nu = 1$ corresponds to about 4.2% of the solar flux received at the surface (Tomasko, 1983). Thus, unless the value of ν is much less than estimated, the wave energy flux involved represents a significant fraction of the total thermal input.

Figure 13 shows profiles of perturbation energy A^2E at z_0. While the spectrum of westerly waves is strongly peaked at the low frequency end, that of easterly waves is comparatively flat and substantially smaller for most frequencies. The integrated values are $3.1\hat{\nu}$ kg m^{-1} s^{-2}

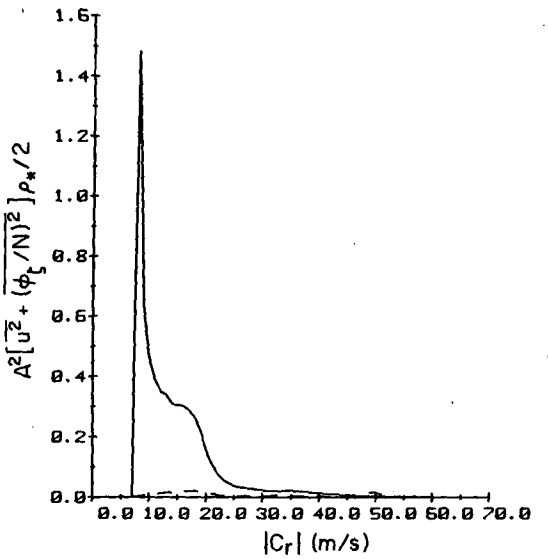

FIG. 13. The perturbation energy density $A^2[\overline{u^2} + (\overline{\phi_z/N_*)^2}]\rho_*/2$ at z_0 in units of kg m^{-1} s^{-2}/(m s^{-1}) scaled by $\hat{\nu}\hat{k}^{-1}$. The solid line is for westerly waves and the dashes for easterly waves.

for westerlies, $0.2\hat{\nu}$ kg m^{-1} s^{-2} for easterlies, giving a total of $3.3\hat{\nu}$ kg m^{-1} s^{-2}, which is negligible compared with the kinetic energy of the mean flow of 963 kg m^{-1} s^{-2} at the same level. The group velocity at the level of excitation is given by $\rho_* \overline{w\phi}/E$; for westerly waves this varies from less than 0.3 m s^{-1} for $c_r \leqslant 20$ m s^{-1} to about 4 m s^{-1} at $c_r = 50$ m s^{-1}; for easterly waves the corresponding values are 0.1 m s^{-1} for $c_r \gtrsim -20$ m s^{-1} and 3 m s^{-1} for $c_r = -50$ m s^{-1}.

In section 2 it was assumed that waves are essentially inviscid away from critical layers; this can now be justified as follows: Figs. 3 and 6 show that the index of refraction Q for both easterly and westerly waves is typically of the order of 10^{-8} m^{-2} (except near the critical level). For the estimated amounts of diffusion, the diffusive time $4\pi^2/(\nu Q)$ for the wave is on the order of years, much greater than the wave transit time (i.e., distance/group velocity), which is typically on the order of hours.

d. *Estimated wave amplitudes*

Substituting (20) into (15) gives $A_{\text{rms}} = 1.1 \times 10^{-2}(\hat{\nu}\hat{k})^{1/2}$, corresponding to a vertical velocity $w = A_{\text{rms}}\tilde{W}$ of $1.1 \times 10^{-2}(\hat{\nu}\hat{k})^{1/2}$ m s^{-1}. At the cloud level this corresponds to about 0.5 m s^{-1} (for $\nu = 5$ m^2 s^{-1}) comparable to the values suggested by VEGA balloon measurements (Linkin et al., 1986). At $z_0 = 10$ km u is less than $1(\hat{\nu}\hat{k})^{1/2}$ m s^{-1} for westerly waves and 10^{-2} m s^{-1} for easterly waves; these values are within data constraints.

As shown in section 4, easterly waves can reach great heights where they are thermally damped, providing that they do not become gravitationally unstable and break down en route. Following Lindzen (1981), the height at which breaking occurs is given by

$$\left|\frac{dT}{dz}\right|_{z_{\text{break}}} = \left(\frac{d\bar{T}}{dz} + \frac{g}{c_p}\right)_{z_{\text{break}}}. \tag{21}$$

For the estimated forcing amplitude of $w(z_0) = 1.1(\hat{\nu}\hat{k})^{1/2}$ cm s^{-1}, the calculated easterly waves do not break for $\hat{k} = 1$ and $\hat{\nu} = 1$, but are thermally damped as described in section 4b. Figure 14 shows the resulting mean-flow deceleration $[\bar{\rho}G]$ attains a maximum of $-1.5 \times 10^{-7}\hat{\nu}$ kg m^{-2} s^{-2} at 93 km. Hou and Goody (1985) have shown that at these heights eddy sinks are required so as to maintain the negative zonal wind shear in the presence of a direct meridional circulation, the estimated deceleration due to damped easterly waves is of the same order as that suggested by Hou and Goody. From Fig. 14 we obtain that the deceleration per unit mass at 90 km is about -30 m s^{-1} day^{-1} ($\hat{\nu} = 1$), which is roughly twice the equatorial deceleration due to the semidiurnal tide at this level, as computed by Valdes (1984). However, given that the exact zonal wind profile is uncertain at these heights, these differences are not significant since the mean wind can adjust itself to the total deceleration. The important conclusion is that gravity waves can provide an additional momentum sink at these altitudes, as they do in the earth's atmosphere.

If easterly waves do propagate to great heights as indicated by these calculations, their amplitudes should be measurable. From Fig. 7a we estimate that u could be as large as $20(\hat{\nu}\hat{k})^{1/2}$ m s^{-1} at 100 km, decreasing rapidly to less than $3(\hat{\nu}\hat{k})^{1/2}$ m s^{-1} for $z \leqslant 80$ km.

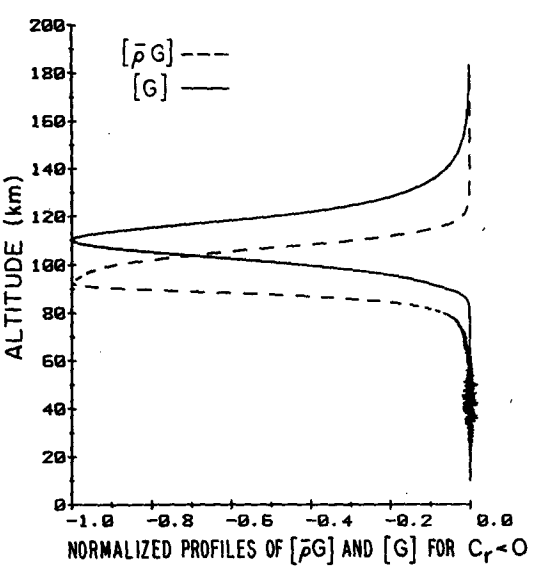

FIG. 14. Total mean-flow deceleration due to easterly waves. The profiles are normalized with respect to maximum values. The dashes show $[\bar{\rho}G(z)]$ scaled by 1.5×10^{-7} kg m^{-2} s^{-2}, and the solid line gives $[G(z)]$ scaled by 320 m s^{-1}/day.

The calculated temperature perturbation is about $10(\hat{\nu}\hat{k})^{1/2}$ K at 100 km and less than $1.5(\hat{\nu}\hat{k})^{1/2}$ K below 80 km, which is within the limits of fluctuation amplitudes in the observed profiles. As already mentioned, the cloud-level vertical velocity is about 0.5 m s^{-1}, comparable to the value of 1 m s^{-1} indicated by the recent Soviet Vega balloon measurements (Linkin et al., 1986); the periods of these waves are longer than several hours, which may be relevant to the trapped gravity waves discussed by Woo et al. (1980).

In these calculations easterly waves do not break in the small static stability region around 55 km (see Fig. 1) because the model static stability is small but positive. From (6) we see that $T \sim N_*^2 \sim S$, so that S cancels in (21); hence a wave does not break simply because S is small. However, at a larger value of ν or if S is identically zero at 55 km, all easterly waves would break at this level, in which case we can distribute the total easterly momentum flux of $-0.6 \times 10^{-2}\hat{\nu}$ kg m^{-1} s^{-2} (see section 5b) over a scale height of 7 km to obtain the estimate $[\bar{\rho}G] \approx -8 \times 10^{-7}\hat{\nu}$ kg m^{-2} s^{-2} (Lindzen, 1981). This is of the same order as the equatorial tidal acceleration at the maximum heating level at 65 km (see Fig. 4.42 of Pechmann, 1983, Fig. 3.36 of Valdes, 1985, and Fels, 1986). Thus, the breaking of easterly waves around 55 km would result in an eddy momentum sink just below the maximum tidal acceleration. Such a layered structure of eddy sources and sinks could be maintained by multiple meridional cells, as discussed in Hou (1984) and Hou and Goody (1985).

A likely situation in the Venus atmosphere may well be a mixture of the two, with easterly waves penetrating to great heights at times and breaking at the mid-cloud level at others.

6. Sensitivity tests

a. Wavenumber dependence

As a result of the long thermal damping time below the cloud base, w is independent of k for westerly waves and the dependence of the various quantities on k may be derived explicitly from (6)–(9), (11), and (20). In particular, from (20) the inverted spectral density $A^2(c)$ is proportional to k, so that $[\rho_*\overline{wu}]$, $[\rho_*\overline{w\phi}]$, and $[\bar{\rho}G]$, are independent of k, while $[E]$ varies as k^{-1} and A_{rms} varies as $k^{1/2}$. The solution for westerly waves can, therefore, be conveniently scaled.

However, the solution for easterly waves is a function of wavenumber since the deposition of the easterly momentum flux is affected by the thermal damping term in (4), which is proportional to k. The results for a 500 km wave ($\hat{k} = 2$) show that the total deceleration $[\bar{\rho}G]$ due to easterly waves is similar in structure to the reference case shown in Fig. 14, but has a maximum of $-0.6 \times 10^{-7}\hat{\nu}$ kg m^{-2} s^{-2} at 103 km. This smaller maximum reflects the decrease in density over two scale heights, which more than offsets the increase with k through A^2 and damping.

b. Sensitivity to the static stability near 24 km

Pioneer Venus data indicate a close-to-neutral layer around 25 km (Schubert, 1983). The measured instantaneous static stability varies from about 0.3 K km^{-1} near the equator to slightly unstable profiles at higher latitudes, with uncertainties of about 0.3 K km^{-1}. Since the momentum supply at the equator, where the atmospheric angular momentum reaches a maximum, is a key issue in the superrotation problem, as argued in Hou (1984), we have assumed an equatorial orientation throughout this study and adopted the equatorial $S(z)$ profile in section 5. However, if the mean static stability in this region is actually zero (or even unstable), waves would break and the proposed mechanism cannot operate for $c_r > c_r(z = 25 \text{ km}) \approx 30$ m s^{-1}. Perhaps, a more interesting question is to ask whether waves could propagate through a low static stability region without breaking, regardless of the value of S, so long as it is positive. To test this, we used an alternate $S(z)$ with a minimum of 7×10^{-2} K km^{-1} at 23.7 km (by setting $\hat{a}_3 = -3.4$ km^{-1} K) and repeated the calculations.

For westerly waves with critical levels in the region of low static stability, the waves break just below the critical level, well within the viscous layer for $\hat{\nu}$ of the order of unity. The easterly waves again do not break. As discussed in section 5, since T is proportional to S, waves do not necessarily break when S is small. Figure 15 shows that the inverted spectral density does not differ greatly from the reference case. Of the various integrated quantities, only $[\rho_*\overline{wu}]$ and $[\rho_*w\phi]$ for easterly waves increase by about 30%. The amplification peak at -5 m s^{-1} shown in Fig. 9 is shifted to -3 m s^{-1}, suggesting that this particular amplification peak is probably due to the rapid variation around the minimum in S at 24 km.

c. Sensitivity to the forcing level

To test the sensitivity to the excitation level, we performed calculations for $z_0 = 5$ km instead of 10 km as in section 5. Figure 15 shows that the spectral density is little altered. Since the containment distance for partially reflected waves depends on the height z_0, the amplification peak at $c_r \approx -5$ m s^{-1} in the reference case is shifted to -12 m s^{-1}, but the one at $c_r \approx -50$ m s^{-1} is not noticeably affected.

7. Discussion and conclusion

We have shown that the prevailing westerlies in the Venus atmosphere introduce a strong bias in favor of the transport of westerly momentum upward by large-scale gravity waves excited near the surface. A continuous spectrum of gravity waves with westerly phase speeds and critical levels below the cloud base could provide the necessary acceleration to maintain the superrotation below 45 km against diffusion (if dynamic transport is as small as suggested by the calculation of

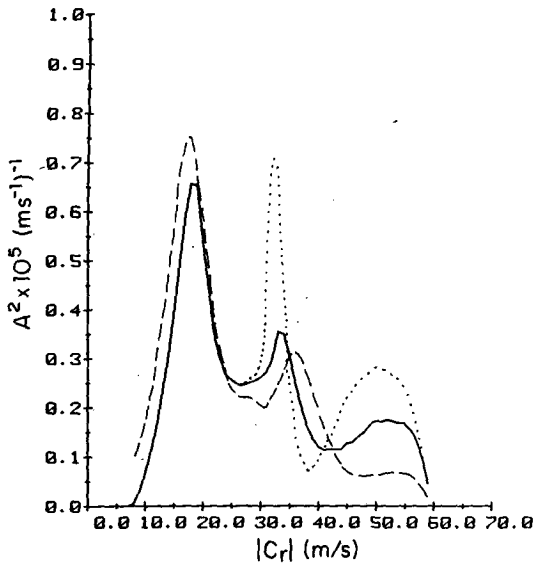

FIG. 15. A comparison of inverted spectral densities from sensitivity tests. The values are scaled by $10^{-5}\bar{\rho}k$. The solid line marks the reference case discussed in section 5, the dashes are for the modified static stability discussed in section 6b, and the dots are for the case $z_0 = 5$ km (see section 6c).

Hou and Goody, 1985). The attendant waves with easterly phase speeds either break at the near-neutral static stability layer around 55 km (if this layer is, in fact, unstable over extended periods) or propagate until absorbed through thermal damping above 80 km. In the event of breaking at 55 km, the resulting mean-flow deceleration may be comparable to the maximum equatorial tidal acceleration at 65 km. Such a layered eddy source/sink structure is consistent with the multiple meridional circulation pattern obtained by Hou and Goody. Alternatively, if easterly waves are thermally damped above 80 km, the resulting deceleration could be comparable to the local tidal deceleration and help provide the required eddy momentum sink to maintain the negative zonal wind shear against the mean meridional transport, as in Hou and Goody.

For the amount of diffusion with ν ranging from 1 to 5 $m^2 s^{-1}$, as suggested by in situ measurements, the estimated wave amplitudes are compatible with observed wind and temperature perturbations. The total vertical wave energy flux is about 0.7–3.5 W m^{-2}, corresponding to 4%–20% of the solar energy flux reaching the planet surface, which implies an extremely efficient energy conversion mechanism. Whether such high efficiencies are easily attainable remains to be demonstrated; however, in view of the uncertainties in the diffusion coefficient, these values may well be overestimates.

A possible candidate for exciting a continuous spectrum of gravity waves is penetrative convection (for example, see Stull, 1976). It has been suggested that small-scale convection may occur in the region of small static stability from 15 to 28 km, or near the surface (Schubert, 1983). The near-zero vertical shear in the zonal wind profile below 10 km may be an additional clue that some vertical mixing is present, which could then excite vertically propagating gravity waves, as suggested by this study. Although there is ample evidence of gravity wave activities in the Venus atmosphere, it is difficult to conclude about the nature of the generation mechanism based on the present-day data. If we assume that convection acts as a random driving, the stipulation that the forced stationary solution presented here is representative of the long-term statistics is valid only if the driving remains coherent for periods that are long compared with wave transit times (travel distance/group velocity); otherwise the long-term statistics may not, for example, exhibit the amplification peaks of the steady solution. However, since the spectral density distribution is the Fourier transform of the autocovariance, the required coherence time of the driving may be estimated by 1/(*e*-folding width of the spectral density); from Fig. 11 we estimate the consistent coherence time to be greater than two wave periods (with the central frequency at $c_r \approx 20$ m s^{-1}), i.e., approximately 30 h. It can be shown that the transit time for the amplification peak at $c_r \approx 50$ m s^{-1} is about 5 h (based on a round-trip distance between 10 to 45 km and an average group velocity of 4 m s^{-1}, see section 5c). However, owing to the small group velocities at the low end of the inverted spectrum and the great depth of their modal structure, transit times for easterly waves in the amplification regions are much longer than the coherence time of the driving. Thus, the results for easterly momentum and energy fluxes (hence the deceleration) for the low frequencies should be regarded as upper-bound estimates, which only serve to further emphasize the east–west asymmetry, which is the basis of the proposed mechanism.

In assuming an equilibrium wind profile with the gravity wave spectrum, we have neglected potential contributions from shear instabilities. However, *Pioneer Venus* data suggest that the Richardson number is greater than 0.25 below the clouds and instabilities are unlikely (Schubert, 1983). For consistency, we have adopted a standard model profile that is stable below 55 km.

Apart from the maintenance question, one might ask whether the proposed mechanism could have caused the superrotation on Venus. Since the differential solar heating has a maximum at the equator, any redistribution of the atmospheric angular momentum by a thermally direct circulation from the state of rest would give rise to westerlies away from the equator, thereby introducing an initial bias in the direction of the planetary rotation, which could then be amplified by the gravity wave mechanism.

However, the primary objective of this work is to propose a simple mechanism for the Venus superro-

tation below 45 km that is consistent with current data, to offer a quantitative assessment of its viability, and to provide a focal point for future observational efforts. Since the root-mean-square amplitude and the momentum flux of large-scale gravity waves are measurable quantities, there is hope that the proposed mechanism could someday be tested.

Acknowledgments. We thank R. S. Lindzen and R. M. Goody for helpful comments. This work was supported by NASA Grant NGL-22-007-228.

REFERENCES

Blumen, W., and C. S. Hartsouth, 1985: Reflection of hydrostatic gravity waves in a stratified shear flow. Part II: Application to downslope surface windstorms. *J. Atmos. Sci.*, **42**, 2319–2331.

Covey, C., and G. Schubert, 1982: Planetary-scale waves in the Venus atmosphere. *J. Atmos. Sci.*, **39**, 2397–2413.

Fels, S. B., 1986: An approximate analytical method for calculating tides in the atmosphere of Venus. *J. Atmos. Sci.*, **43**, 2757–2772.

——, and R. S. Lindzen, 1974: The interaction of thermally excited gravity waves with mean flows. *Geophys. Fluid Dyn.*, **6**, 149–192.

Fritts, D. C., and M. A. Geller, 1976: Viscous stabilization of gravity wave critical level flows. *J. Atmos. Sci.*, **33**, 2276–2284.

Gill, A. E., 1982: *Atmospheric–Ocean Dynamics.* Academic Press, 662 pp.

Gold, T., and S. Soter, 1971: Atmospheric tides and the 4-day circulation on Venus. *Icarus*, **14**, 16–20.

Hazel, P., 1967: The effect of viscosity and heat conduction on internal gravity waves at a critical level. *J. Fluid Mech.*, **30**, 775–784.

Holton, J. R., 1975: *The Dynamic Meteorology of the Stratosphere and Mesosphere.* Amer. Meteor. Soc., 216 pp.

Hou, A. Y., 1984: Axisymmetric circulations forced by heat and momentum sources: A simple model applicable to the Venus atmosphere. *J. Atmos. Sci.*, **41**, 3437–3455.

——, and R. M. Goody, 1985: Diagnostic requirements for the superrotation on Venus. *J. Atmos. Sci.*, **42**, 413–432.

Klemp, J. B., and D. Lilly, 1975: The dynamics of wave-induced downslope winds. *J. Atmos. Sci.*, **32**, 320–339.

Lindzen, R. S., 1970: Internal gravity waves in atmospheres with realistic dissipation and temperature. Part I. Mathematical development and propagation of waves into the thermosphere. *Geophys. Fluid Dyn.*, **1**, 303–355.

——, 1981: Turbulence and stress owing to gravity wave and tidal breakdown. *J. Geophys. Res.*, **86**, 9707–9714.

——, and J. W. Barker, 1985: Instability and wave over-reflection in stably stratified shear flow. *J. Fluid Mech.*, **151**, 189–217.

——, and J. R. Holton, 1968: A theory of the quasi-biennial oscillation. *J. Atmos. Sci.*, **25**, 1095–1107.

——, and K. K. Tung, 1976: Banded convective activity and ducted gravity waves. *Mon. Wea. Rev.*, **104**, 1602–1617.

Linkin, V. M., V. V. Kerzhanovich, A. N. Lipator, K. M. Pichkadze, A. A. Shurupov, A. V. Terterashvili, A. P. Ingersoll, D. Crisp, A. W. Grossman, R. E. Young, A. Seiff, B. Ragent, J. E. Blamont, L. S. Elson and R. A. Preston, 1986: VEGA balloon dynamics and vertical winds in the Venus middle cloud region. *Science*, **231**, 1417–1419.

Malkus, V. W. R., 1970: Hadley–Halley circulation on Venus. *J. Atmos. Sci.*, **27**, 529–535.

Pechmann, J., 1983: Thermal tides in the atmosphere of Venus. Ph.D. thesis, California Institute of Technology, 286 pp.

Plumb, A., 1977: The interaction of two internal waves with the mean flow: Implications for the theory of quasi-biennial oscillation. *J. Atmos. Sci.*, **34**, 1847–1858.

Pollack, J. B., and R. Young, 1975: Calculations of the radiative and dynamical state of the Venus atmosphere. *J. Atmos. Sci.*, **32**, 1025–1037.

Schubert, G., 1983: General circulation and the dynamical state of the Venus atmosphere. *Venus*, D. M. Hunten et al., Eds., The University of Arizona Press, 681–765.

——, and R. L. Waltercheid, 1984: Propagation of small-scale acoustic-gravity waves in the Venus atmosphere. *J. Atmos. Sci.*, **41**, 1202–1213.

——, and J. Whitehead, 1969: Moving flame experiment with liquid mercury: Possible implications for the Venus atmosphere. *Science*, **163**, 71–72.

Seiff, A., 1983: Thermal structure of the atmosphere of Venus. *Venus*, D. M. Hunten et al., Eds., The University of Arizona Press, 215–279.

Stull, R. B., 1976: Internal gravity waves generated by penetrative convection. *J. Atmos. Sci.*, **33**, 1279–1286.

Thompson, R., 1970: Venus' general circulation is a merry-go-round. *J. Atmos. Sci.*, **27**, 1107–1116.

Tomasko, M. G., 1983: The thermal balance of the lower atmosphere of Venus. *Venus*, D. M. Hunten et al., Eds., The University of Arizona Press, 604–631.

Valdes, P., 1984: Large-scale waves in the atmosphere of Venus. Ph.D. thesis, Oxford University, 400 pp.

von Zahn, U., S. Kumar, H. Niemann and R. Previn, 1983: Composition of the Venus atmosphere. *Venus*, D. M. Hunten et al., Eds., The University of Arizona Press, 299–430.

Woo, R., J. W. Armstrong and A. Ishimaru, 1980: Radio occultation measurements of turbulence in the Venus atmosphere by *Pioneer Venus. J. Geophys. Res.*, **85**, 8031–8038.

Young, R. E., and G. Schubert, 1973: Dynamical aspects of the Venus 4-day circulation. *Planet. Space Sci.*, **21**, 1563–1580.